1-1-2014

Ni-Doped $Sr_2Fe_{1.5}Mo_{0.5}O_{6-\delta}$ as Anode Materials for Solid Oxide Fuel Cells

Guoliang Xiao

Siwei Wang

Ye Lin
University of South Carolina - Columbia, linye@mailbox.sc.edu

Zhibin Yang

Minfang Han
University of South Carolina - Columbia

See next page for additional authors

Publication Info

Published in *Journal of The Electrochemical Society*, Volume 151, Issue 3, 2014, pages F805-F810.

Publisher's Version: http://dx.doi.org/10.1149/2.061403jes
Xiao, G., Wang, S., Lin, Y., Yang, Z., Han, M., & Chen, F. (1 January 2014). Ni-Doped $Sr_2Fe_{1.5}Mo_{0.5}O_{6-\delta}$ as Anode Materials for Solid Oxide Fuel Cells. Journal of The Electrochemical Society, 151 (3), F805 – F810. http://dx.doi.org/10.1149/2.061403jes

Journal of The Electrochemical Society, **161** (3) F305-F310 (2014)
0013-4651/2014/161(3)/F305/6/$31.00 © The Electrochemical Society

Ni-doped $Sr_2Fe_{1.5}Mo_{0.5}O_{6-\delta}$ as Anode Materials for Solid Oxide Fuel Cells

Guoliang Xiao,[a] Siwei Wang,[a,*] Ye Lin,[a] Zhibin Yang,[b] Minfang Han,[b,z] and Fanglin Chen[a,,z]**

[a]*Department of Mechanical Engineering, University of South Carolina, Columbia, South Carolina 29208, USA*
[b]*School of Chemical and Environment Engineering, China University of Mining and Technology, Beijing 100083, China*

10% Ni-doped $Sr_2Fe_{1.5}Mo_{0.5}O_{6-\delta}$ with A-site deficiency is prepared to induce in situ precipitation of B-site metals under anode conditions in solid oxide fuel cells. XRD, SEM and TEM results show that a significant amount of nano-sized Ni-Fe alloy metal phase has precipitated out from $Sr_{1.9}Fe_{1.4}Ni_{0.1}Mo_{0.5}O_{6-\delta}$ upon reduction at 800°C in H_2. The conductivity of the reduced composite reaches 29 S cm^{-1} at 800°C in H_2. Furthermore, fuel cell performance of the composite anode $Sr_{1.9}Fe_{1.4}Ni_{0.1}Mo_{0.5}O_{6-\delta}$-SDC is investigated using H_2 as fuel and ambient air as oxidant with $La_{0.8}Sr_{0.2}Ga_{0.87}Mg_{0.13}O_3$ electrolyte and $La_{0.6}Sr_{0.4}Co_{0.2}Fe_{0.8}O_3$ cathode. The cell peak power density reaches 968 mW cm^{-2} at 800°C and the voltage is relatively stable under a constant current load of 0.54 A cm^{-2}. After 5 redox cycles of the anode at 800°C, the fuel cell performance doesn't suffer any degradation, indicating good redox stability of $Sr_{1.9}Fe_{1.4}Ni_{0.1}Mo_{0.5}O_{6-\delta}$. Peak power density of 227 mW cm^{-2} was also obtained when propane is used as fuel. These results indicate that a self-generated metal-ceramic composite can been successfully derived from $Sr_2Fe_{1.5}Mo_{0.5}O_{6-\delta}$ by compositional modifications and $Sr_{1.9}Fe_{1.4}Ni_{0.1}Mo_{0.5}O_{6-\delta}$ is a very promising solid oxide fuel cell anode material with enhanced catalytic activity and inherited good redox stability from the parent ceramic material.
 [DOI: 10.1149/2.061403jes]

Manuscript submitted November 8, 2013; revised manuscript received December 6, 2013. Published January 1, 2014. This was Paper 760 presented at the San Francisco, CA, Meeting of the Society, October 27-November 1, 2013.

Ceramic anode materials have drawn a lot of attention due to their potentially better stability in different fuels or under redox cycling in solid oxide fuel cells (SOFCs) comparing with the conventional Ni-based cermet anodes. Among the proposed ceramic anode candidates, perovskite-type oxides, such as $LaCrO_3$-based and $SrTiO_3$-based materials, have been intensively studied due to their relatively high mixed conductivity and good stability in reducing atmospheres.[1–4] Recently, a new class of $Sr_2M_{1-x}Mo_xO_{6-\delta}$ materials (M = Mn, Fe, Co, Ni, $0 < x < 1$) with double perovskite structure have been demonstrated as anode materials for SOFCs.[5–9] This type of material has various B-site cation choices in a wide range of compositions, offering flexibility in tuning their properties. Several interesting anode candidates with this structure have been reported with good stability in different fuels and under redox cycling.[6,9]

Ceramic anode materials exhibit good stability but there are still considerable needs for improving their overall cell performance. One of the limiting properties of these ceramic candidates is their relatively low catalytic activity. Many studies have shown that the fuel cell performance can be dramatically improved by introducing a small amount of metal catalysts to these mixed conductors.[10–14] Unlike the cermet materials which require a large volume ratio of the metal phase to provide percolating conductive passage, it is possible to fabricate highly dispersed metal catalyst on the mixed-conducting ceramic backbones. With good mixed conducting properties, the ceramic materials may help stabilizing the metallic catalyst phase, promoting their catalytic activity and eventually mitigating the instability issues that cermet anodes typically have. Several reports have demonstrated both enhanced activity and stability of the metal modified ceramic anode materials.[11,13,14]

Regarding the modification method, infiltration is always an easy and effective way to obtain the supported catalysts on porous substrates and many reported metal modified ceramic anodes have been prepared by this approach as mentioned above. Recently, in situ generation of metal particles from oxides has been considered as an alternative way to obtain the supported metal catalysts in certain oxide material systems.[15–19] Compared with the infiltration approach, in situ generation of metal particles is much simpler and is less affected by other factors such as the morphology of the ceramic backbones. The size and loading amount of the metal particles are determined by the chemical properties of the oxides and the metallic catalyst distribution may be more homogeneous since the metals are precipitated directly from the ceramic lattice. Nano-sized Ni, Ru, and Pd particles have been reported to be uniformly dispersed on oxides via reduction of $LaCrO_3$- or $NbTi_{0.5}Ni_{0.5}O_4$- based materials and enhanced fuel cell performance has been observed with these composite anode materials.[15–18] By exposing $Pr_{0.4}Sr_{0.6}Co_{0.2}Fe_{0.7}Nb_{0.1}O_3$ to a reducing environment at 900°C, nano-sized Co-Fe alloy particles supported on a ceramic matrix have been obtained. Besides the enhanced anode activity, an interesting regenerative behavior upon in situ redox cycling has also been achieved in this material system.[19]

Previously, we have successfully improved $Sr_2Fe_{1.5}Mo_{0.5}O_{6-\delta}$ anode performance by incorporating a small amount of Ni through infiltration.[13,14] Since Ni shows good catalytic activity and can be more easily reduced than Fe, in this study we substitute Fe on the B-site of $Sr_2Fe_{1.5}Mo_{0.5}O_{6-\delta}$ with 10% Ni and expect to in situ generate metal-ceramic composite anode under the fuel cell operating conditions. By introducing slight A-site deficiency, precipitation of metal particles on the ceramic matrix has been facilitated. The electrochemical performance and stability of the obtained composite anode are systematically studied.

Experimental

Material synthesis.— $Sr_2Fe_{1.4}Ni_{0.1}Mo_{0.5}O_{6-\delta}$ and $Sr_{1.9}Fe_{1.4}Ni_{0.1}Mo_{0.5}O_{6-\delta}$ were prepared by a combustion process. Stoichiometric amount of $(NH_4)_6Mo_7O_{24}$ $4H_2O$ was first dissolved in deionized water. To prepare 0.01 mole of the oxide, 2g of citric acid was then added to the solution as a chelating agent to prevent precipitation of the molybdate salt. $Sr(NO_3)_2$, $Fe(NO_3)_3$ $9H_2O$ and $Ni(NO_3)_2$ $6H_2O$ were then dissolved and a clear yellowish solution was formed. Finally, 15g of glycine was added as a combustion agent and the solution turned dark red. The as-prepared solution was heated by a microwave oven with 1000 W power until self-ignition took place. The ash was then collected and heat-treated at 1100°C in air for 5 h to form the perovskite structure. The interlayer material $La_{0.4}Ce_{0.6}O_2$ (LDC) and the cathode material $La_{0.6}Sr_{0.4}Co_{0.2}Fe_{0.8}O_3$ (LSCF) were prepared by a similar citric acid-assisted combustion method. $La_{0.8}Sr_{0.2}Ga_{0.87}Mg_{0.13}O_3$ (LSGM) electrolyte powder was synthesized by solid-state reaction.

Characterization.— XRD patterns of the powders were recorded using a D/MAX-3C X-ray diffractometer with graphite-monochromatized Cu Kα radiation (λ = 1.5418 Å). XPS was

*Electrochemical Society Student Member.
**Electrochemical Society Active Member.
zE-mail:hanminfang@sina.com;chenfa@cec.sc.edu

measured using a Kratos Axis Ultra DLD instrument and spectra were calibrated by C 1s at 284.6 eV. SEM images of the powders before and after reduction were evaluated using a Zeiss Ultra plus Thermal Field Emission Scanning Electron Microscope. The metal-ceramic composite achieved by reducing $Sr_{1.9}Fe_{1.4}Ni_{0.1}Mo_{0.5}O_{6-\delta}$ was also characterized by high-resolution transmission electron microscopy (HRTEM). The powders were dispersed in ethanol and well sonicated before dipped onto Holey Carbon 400 mesh Cu grid (Ted Pella, Inc.). JEOL 3000F with a point-to-point resolution of 0.17 nm operating at 300 kV and JEOL2100F equipped with a Schottky field-emission gun (FEG), with Cs = 1.0 mm operated at 200 kV were used for imaging. EDX tests were carried out in the STEM mode.

$Sr_{1.9}Fe_{1.4}Ni_{0.1}Mo_{0.5}O_{6-\delta}$ was pressed into a rectangular bar ($40 \times 6 \times 2$ mm^3) and sintered at 1300°C for 6h for electrical conductivity measurement. Ag wires and Ag paste were used to attach four probes on the sintered bar sample. The bar with attached Ag wires was placed in a tubular furnace with air or H_2 (3 vol% H_2O) flowing at a rate of 80 mL min^{-1} and the resistance was recorded by a multimeter (Keithley model 2001 7–1/2 DDM) in a dc four-probe configuration from 800 to 400°C. For the conductivity measurement in H_2, the bar was first reduced at 800°C for 10 h before the data was collected.

Cell fabrication and test.— LSGM powder was pressed into pellets and sintered at 1450°C for 10 h to form dense electrolyte membranes. Electrode inks and LDC ink were made by mixing the powders with a Heraeus binder V006 at a weight ratio of 1:1.5. The LDC layer to prevent the reaction between LSGM and Ni from the anode was fabricated by painting the LDC ink on the LSGM electrolyte pellet followed by sintering at 1350°C for 2 h. The anode was then painted on the LDC layer and the cathode was painted on the other side of the LSGM electrolyte pellet. After drying, the electrodes were co-fired in air at 1100°C for 2 h. Au paste and Pt paste were painted on the anode and cathode, respectively and fired at 1000°C for 0.5 h to form the current collector. Two wires were connected to each electrode and the cells were tested in a four-probe configuration. The flow rate of the fuel gas was set to 40 mL min^{-1} and ambient air was used as oxidant. A Versa STAT 3–400 test system (Princeton Applied Research) was used for electrochemical characterizations. For electrochemical impedance measurements, 10 mV of *ac* perturbation was applied and impedance spectra were measured from 10^6 Hz to 0.02 Hz.

Results and Discussion

Pure cubic perovskite phases of $Sr_2Fe_{1.4}Ni_{0.1}Mo_{0.5}O_{6-\delta}$ and $Sr_{1.9}Fe_{1.4}Ni_{0.1}Mo_{0.5}O_{6-\delta}$ can be obtained by firing the precursors at 1100°C in air for 5 h. As shown in Figure 1a, no impurity peak was detected in the XRD patterns for both compositions. The only difference is that the XRD peaks of the Sr-deficient one slightly shifted to lower angles as shown in Figure 1b, indicating that the lattice was expanded. The lattice expansion in $Sr_{1.9}Fe_{1.4}Ni_{0.1}Mo_{0.5}O_{6-\delta}$ is consistent with those reported for A-site deficient composites in other

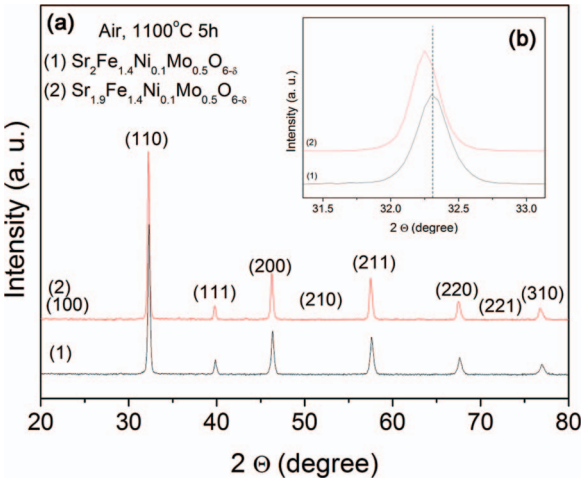

Figure 1. a) XRD pattern of $Sr_2Fe_{1.4}Ni_{0.1}Mo_{0.5}O_{6-\delta}$ and $Sr_{1.9}Fe_{1.4}Ni_{0.1}Mo_{0.5}O_{6-\delta}$ synthesized in air at 1100°C, and b) enlarged (110) peak.

Table I. Lattice constant and crystalline size calculated from XRD pattern.

	Lattice Constant (Å)	Crystalline size (nm)*
$Sr_{1.9}Fe_{1.4}Ni_{0.1}Mo_{0.5}O_{6-\delta}$	3.9243(6)	42.6(9)
$Sr_2Fe_{1.4}Ni_{0.1}Mo_{0.5}O_{6-\delta}$	3.9195(5)	33.2(8)

*Based on FWHM of (110) peak.

systems.[20] The cation deficiency can be accompanied by generating oxygen vacancies and p-type defects in the lattice for charge compensation. The general decrease in oxygen content results in the lattice expansion in these A-site deficient composites. The lattice parameters and crystalline sizes of both samples were calculated by Jade software and listed in Table I. Larger crystalline particles were obtained for $Sr_{1.9}Fe_{1.4}Ni_{0.1}Mo_{0.5}O_{6-\delta}$, indicating the A-site deficient sample is also easier to be sintered, consistent with other reports.[21] The lattice parameter of $Sr_2Fe_{1.4}Ni_{0.1}Mo_{0.5}O_{6-\delta}$ is slightly smaller than that of $Sr_2Fe_{1.5}Mo_{0.5}O_{6-\delta}$ due to the p-type doping of Ni which also increases the concentration of Fe^{4+}, the p-type defects.

In order to verify the impact of p-type doing of Ni on the oxidation state of Fe, XPS was conducted for $Sr_2Fe_{1.5}Mo_{0.5}O_{6-\delta}$, $Sr_2Fe_{1.4}Ni_{0.1}Mo_{0.5}O_{6-\delta}$ and $Sr_{1.9}Fe_{1.4}Ni_{0.1}Mo_{0.5}O_{6-\delta}$ and the Fe 2p core levels are shown in Figure 2. Previously, the Fe oxidation states in a series of Mo-doped $SrFeO_{3-\delta}$ have been analyzed by fitting Fe 2p 3/2 signal with three interval-fixed peaks, which are assumed to correspond to Fe^{4+}, Fe^{3+} and Fe^{2+}, respectively.[22] The estimated results are well consistent with the observation from neutron diffraction. Considering the similar material compositions, the fitting model was

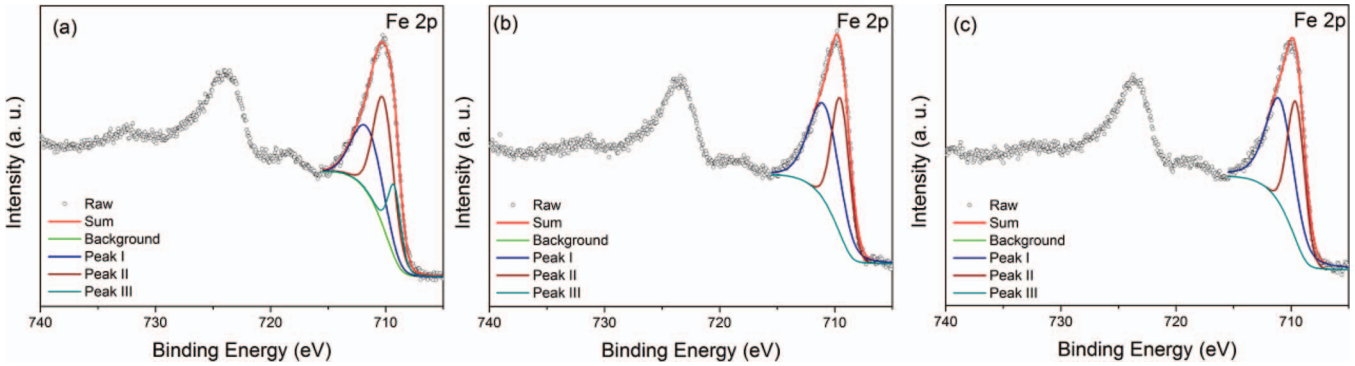

Figure 2. Fe 2p core levels of (a) $Sr_2Fe_{1.5}Mo_{0.5}O_{6-\delta}$, $Sr_2Fe_{1.4}Ni_{0.1}Mo_{0.5}O_{6-\delta}$ and $Sr_{1.9}Fe_{1.4}Ni_{0.1}Mo_{0.5}O_{6-\delta}$.

Table II. Fitting results for Fe 2p 3/2 signal.

	Binding Energy (eV)			Area Ratio (%)				
	I	II	III	I	II	III	Oxidation State of Fe	Oxygen Content
$Sr_2Fe_{1.5}Mo_{0.5}O_{6-\delta}$	711.58	710.17	709.24	33.94	48.02	18.04	3.16	5.87
$Sr_2Fe_{1.4}Ni_{0.1}Mo_{0.5}O_{6-\delta}$	710.89	709.48	708.55	56.77	43.23	0	3.57	5.81
$Sr_{1.9}Fe_{1.4}Ni_{0.1}Mo_{0.5}O_{6-\delta}$	710.96	709.55	708.62	59.76	40.24	0	3.60	5.71

directly applied in this work as well. The fitting results are shown in Table II. The fitting peak III corresponding to Fe^{2+} is reduced significantly in both Ni-doped samples, indicating a p-type electronic compensation mechanism for Ni-doping and resulting in an increase in oxidation state of Fe. It can be noted that the oxidization state of Fe is even slightly higher in $Sr_{1.9}Fe_{1.4}Ni_{0.1}Mo_{0.5}O_{6-\delta}$ than that in $Sr_2Fe_{1.4}Ni_{0.1}Mo_{0.5}O_{6-\delta}$ due to the partial electronic charge compensation for the cation deficiency as discussed above. According to the average oxidation state of Fe and assuming that Ni^{2+} and Mo^{6+} occur in the oxide in oxidizing atmosphere, the oxygen content for each composition can be estimated and the results are also listed in Table II. The value for $Sr_2Fe_{1.5}Mo_{0.5}O_{6-\delta}$ is consistent with those reported elsewhere.[22,23] The oxygen content is 5.81 for $Sr_2Fe_{1.4}Ni_{0.1}Mo_{0.5}O_{6-\delta}$ and 5.71 for $Sr_{1.9}Fe_{1.4}Ni_{0.1}Mo_{0.5}O_{6-\delta}$, which are in agreement with our expectations.

Figure 3 shows the XRD patterns of $Sr_2Fe_{1.4}Ni_{0.1}Mo_{0.5}O_{6-\delta}$ and $Sr_{1.9}Fe_{1.4}Ni_{0.1}Mo_{0.5}O_{6-\delta}$ after reduction at 800°C in H_2 (3vol% H_2O) for 10 h. Besides the major perovskite phase, secondary phases were also detected in the reduced samples. By contrast, the un-doped $Sr_2Fe_{1.5}Mo_{0.5}O_{6-\delta}$ still showed pure perovskite phase under similar treatments as observed in our previous work.[6] The Gibbs free energy for reduction of Ni oxide and Fe oxide at 800°C were calculated using the HSC Chemistry program and listed below.

$$NiO_{(s)} + H_{2(g)} = Ni_{(s)} + H_2O_{(g)} \quad \Delta G = -46.5\,kJ\,mol^{-1} \qquad [1]$$

$$\frac{1}{2}Fe_2O_{3(s)} + \frac{3}{2}H_{2(g)} = Fe_{(s)} + \frac{3}{2}H_2O_{(g)} \quad \Delta G = -12.5\,kJ\,mol^{-1} \qquad [2]$$

From Eq. 1 and Eq. 2, it can be seen that both reduction reactions are thermodynamically favorable in typical SOFC anode conditions but Ni oxide is much easier to be reduced than Fe oxide. The high oxidation state of transition metal cations can be stabilized when forming a perovskite structure. In our previous work, we observed that Mo-doping in $Sr_2Fe_{1.5}Mo_{0.5}O_{6-\delta}$ further improved its stability in reducing atmospheres and no metal Fe was formed under the SOFC operating conditions. However, substitution of Ni for Fe may reduce the stability of $Sr_2Fe_{1.5}Mo_{0.5}O_{6-\delta}$. The stability of several double perovskite anode materials has recently been systematically investigated, in which good chemical stability of $Sr_2Fe_{1.5}Mo_{0.5}O_{6-\delta}$ and decomposition of $Sr_2NiMoO_{6-\delta}$ in reducing conditions have been reported.[24] The decrease of phase stability in reducing atmospheres triggered metal phase formation in Ni-doped $Sr_2Fe_{1.5}Mo_{0.5}O_{6-\delta}$. The cubic Ni-Fe alloy phase (JCDPS#41–1417) was detected in both samples after reduction as shown in Figure 3. However, in the stoichiometric composition, once the Ni-Fe phase starts to precipitate, excess Sr on the A-site may cause formation of some Sr-rich phase, shown as a shoulder peak at around 31 degree, which may inhibit further formation of the metal phase. Therefore, the intensity of Ni-Fe alloy phase was very low in $Sr_2Fe_{1.4}Ni_{0.1}Mo_{0.5}O_{6-\delta}$ while the metal precipitation is significantly enhanced in $Sr_{1.9}Fe_{1.4}Ni_{0.1}Mo_{0.5}O_{6-\delta}$ with A-site deficiency. The exact composition of the Sr-rich impurity phase was not determined due to the low intensity.

Morphology change upon reduction of $Sr_{1.9}Fe_{1.4}Ni_{0.1}Mo_{0.5}O_{6-\delta}$ was further investigated by SEM. Figure 4a shows the SEM image of $Sr_{1.9}Fe_{1.4}Ni_{0.1}Mo_{0.5}O_{6-\delta}$ after being fired at 1100°C in air. Typical sponge-like powder made by combustion methods with smooth and well crystallized surface can be observed. The powder surface became fairly rough upon reduction as shown in Figure 4b. With an enlarged image and in the areas circled in Figure 4c, it can be seen that a lot of nano-sized metal particles with diameters arranging from 10 to 50 nm have been formed on the surface, as detected by XRD. An SEM image of $Sr_2Fe_{1.5}Mo_{0.5}O_{6-\delta}$ after being reduced under the similar condition is shown in Figure 4d for comparison. No evident surface change can be observed which is consistent with the XRD results in our previous report, indicating the better phase stability of $Sr_2Fe_{1.5}Mo_{0.5}O_{6-\delta}$ in reducing atmosphere.[6]

In order to verify the metal phase location in reduced $Sr_{1.9}Fe_{1.4}Ni_{0.1}Mo_{0.5}O_{6-\delta}$, HRTEM was conducted on powders before and after reduction and the images are shown in Figure 5. In

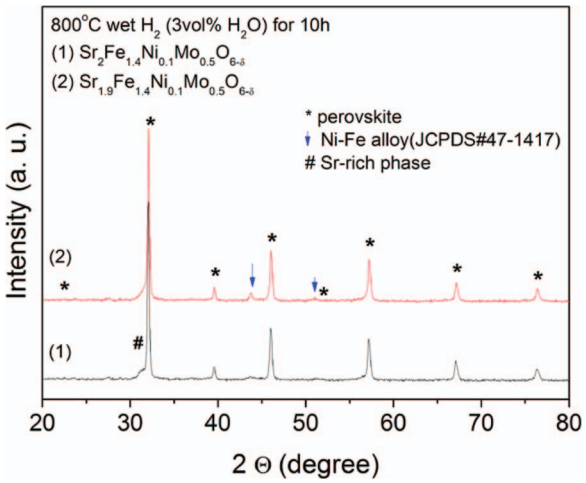

Figure 3. XRD pattern of $Sr_2Fe_{1.4}Ni_{0.1}Mo_{0.5}O_{6-\delta}$ and $Sr_{1.9}Fe_{1.4}Ni_{0.1}Mo_{0.5}O_{6-\delta}$ after reduction in H_2 (3 vol% H_2O) at 800°C for 10 h.

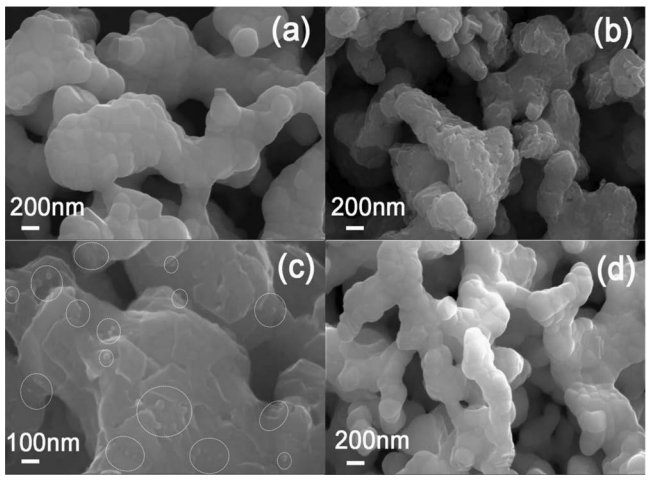

Figure 4. SEM images of (a) $Sr_{1.9}Fe_{1.4}Ni_{0.1}Mo_{0.5}O_{6-\delta}$ synthesized in air, (b), (c) reduced $Sr_{1.9}Fe_{1.4}Ni_{0.1}Mo_{0.5}O_{6-\delta}$ in different magnifications with some of the particles circulated, and (d) $Sr_2Fe_{1.5}Mo_{0.5}O_{6-\delta}$ reduced in H_2 (3 vol% H_2O) at 800°C for 10 h.

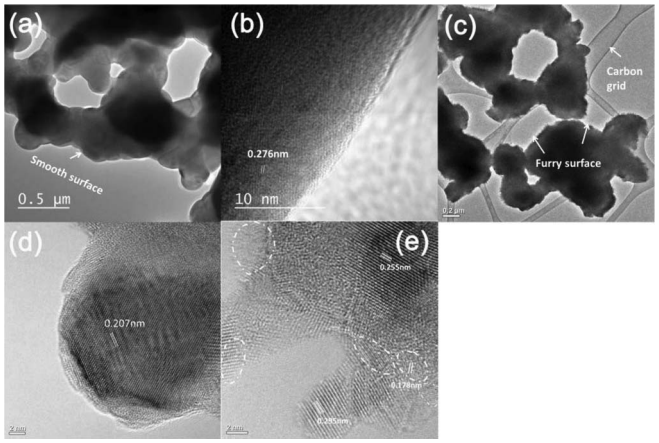

Figure 5. (a) Bright field TEM image and (b) HRTEM image of $Sr_{1.9}Fe_{1.4}Ni_{0.1}Mo_{0.5}O_{6-\delta}$, (c) Bright field TEM image of reduced $Sr_{1.9}Fe_{1.4}Ni_{0.1}Mo_{0.5}O_{6-\delta}$, HRTEM image of (d) a typical metal alloy particle and (e) the furry surface of reduced $Sr_{1.9}Fe_{1.4}Ni_{0.1}Mo_{0.5}O_{6-\delta}$.

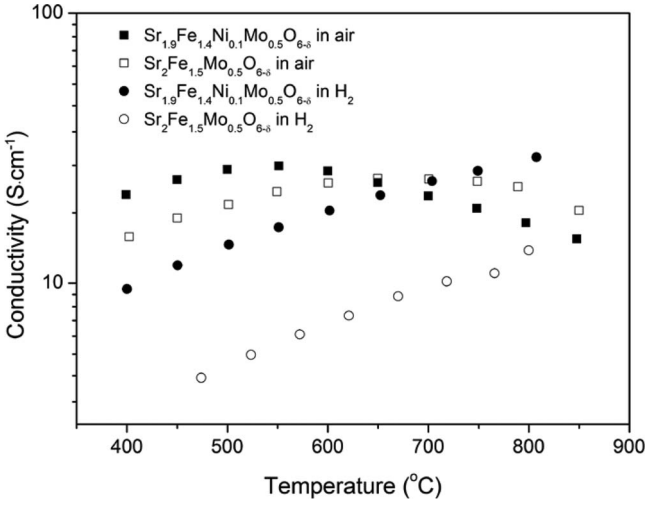

Figure 6. Electrical conductivity of $Sr_{1.9}Fe_{1.4}Ni_{0.1}Mo_{0.5}O_{6-\delta}$ (solid) and $Sr_2Fe_{1.5}Mo_{0.5}O_{6-\delta}$ (open).

accordance with the SEM observation, bright field TEM image of $Sr_{1.9}Fe_{1.4}Ni_{0.1}Mo_{0.5}O_{6-\delta}$ before reduction exhibits smooth contours of the particles as seen in Figure 5a. The lattice parameter measured on the HRTEM image in Figure 5b was about 0.276 nm, corresponding to the reflection originating from the perovskite crystal plane (110). Significant morphology change of the reduced $Sr_{1.9}Fe_{1.4}Ni_{0.1}Mo_{0.5}O_{6-\delta}$ is revealed by the furry contours of the powder as shown in the bright field TEM image in Figure 5c. Figure 5d shows the HRTEM image of a typical nano-sized metal alloy particle generated by reduction. The particle size was about 15 nm and the crystal plane (111) of cubic Ni-Fe alloy with d-spacing of 0.207 nm was observed.[25] Figure 5e shows the HRTEM image of the furry surface of the reduced $Sr_{1.9}Fe_{1.4}Ni_{0.1}Mo_{0.5}O_{6-\delta}$. It can be seen that this layer was composed of smaller particles less than 5 nm. Several small zones showing a d-spacing of 0.178 nm, corresponding to (200) plane of the Ni-Fe alloy phase, can be observed. According to EDS analysis, the Ni/Fe ratio is around 10 at% in the furry surface area, higher than that of 5 at% measured in the region beneath the surface, confirming the precipitation trend of Ni during reduction. Besides the metal alloy phase, crystal grains with d-spacing of 0.295 m and 0.255 nm were also determined in Figure 5e in the furry surface area. These planes are probably corresponding to (111) and (200) of cubic SrO (JCDPS #48–1477) which was not detected by XRD due to the low content. It suggests that the reduction also caused slight surface decomposition of $Sr_{1.9}Fe_{1.4}Ni_{0.1}Mo_{0.5}O_{6-\delta}$.

Bulk electrical conductivity of $Sr_{1.9}Fe_{1.4}Ni_{0.1}Mo_{0.5}O_{6-\delta}$ was measured by a dc four-probe method in both air and H_2 and the results are compared with that of $Sr_2Fe_{1.5}Mo_{0.5}O_{6-\delta}$ in Figure 6. Mo-doped $SrFeO_{6-\delta}$ shows a p-type conduction behavior in oxidizing atmospheres.[26] Since Ni-doping and Sr-deficiency can all be considered as p-type doping for $Sr_2Fe_{1.5}Mo_{0.5}O_{6-\delta}$, improved conductivity of $Sr_{1.9}Fe_{1.4}Ni_{0.1}Mo_{0.5}O_{6-\delta}$ was observed below 500°C when the doping was dominantly compensated by electron holes. At higher temperatures, ionic charge compensation by oxygen vacancies started to take effect. Since the oxygen vacancies are easier to form in $Sr_{1.9}Fe_{1.4}Ni_{0.1}Mo_{0.5}O_{6-\delta}$, its conductivity dropped below that of $Sr_2Fe_{1.5}Mo_{0.5}O_{6-\delta}$ when temperature increased. The comparison of conductivity in air between $Sr_{1.9}Fe_{1.4}Ni_{0.1}Mo_{0.5}O_{6-\delta}$ and $Sr_2Fe_{1.5}Mo_{0.5}O_{6-\delta}$ confirms that Ni was well incorporated into the lattice before reduction. However, Mo-content in the ceramic phase will slightly increase for the reduced $Sr_{1.9}Fe_{1.4}Ni_{0.1}Mo_{0.5}O_{6-\delta}$, which will be beneficial to the n-type conductivity, due to the loss of Fe and Ni from the lattice. Together with the conductive metal phase, the conductivity of reduced $Sr_{1.9}Fe_{1.4}Ni_{0.1}Mo_{0.5}O_{6-\delta}$ in H_2 was evidently higher than that of $Sr_2Fe_{1.5}Mo_{0.5}O_{6-\delta}$. Its electrical conductivity reached 29 S cm^{-1} at 800°C, which is sufficient for applying this material in a composite anode of SOFCs.

Single cell performance of $Sr_{1.9}Fe_{1.4}Ni_{0.1}Mo_{0.5}O_{6-\delta}$-SDC composite anode was tested on LSGM electrolyte with a LDC interlayer and LSCF cathode. Figure 7 shows the cell performance as well as the corresponding impedance spectra at 750, 800, and 850°C in H_2. The peak power density at 800°C reached 968 mW cm^{-2} which is evidently higher than that of the cell with $Sr_2Fe_{1.5}Mo_{0.5}O_{6-\delta}$ or $Sr_2Fe_{1.5}Mo_{0.5}O_{6-\delta}$-SDC anodes in similar cell configurations.[27,28] Such improvement can be attributed to the good catalytic activity of the metal alloy phase formed in the anode. However, the fuel cell power output is still lower than that of Ni-modified $Sr_2Fe_{1.5}Mo_{0.5}O_{6-\delta}$ prepared by an infiltration method reported in our previous work.[13,14] It is mainly due to the different amount of effective metal catalysts

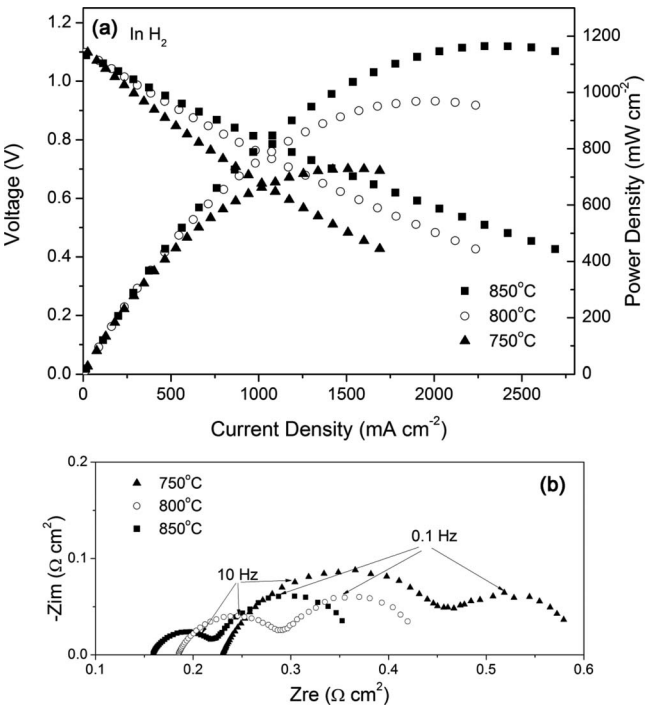

Figure 7. (a) I-V and I-P curves and (b) impedance spectra of $Sr_{1.9}Fe_{1.4}Ni_{0.1}Mo_{0.5}O_{6-\delta}$-SDC anode tested in H_2 (3 vol% H_2O) at 700, 750 and 800°C with LSGM electrolyte and LSCF cathode.

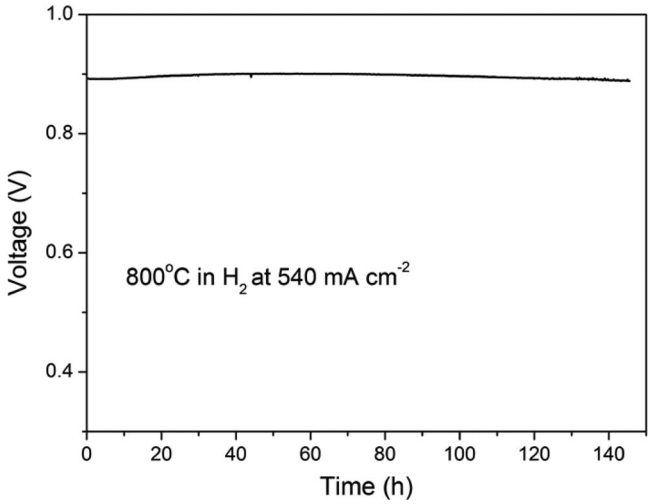

Figure 8. Voltage dependence on time of a single cell with $Sr_{1.9}Fe_{1.4}Ni_{0.1}Mo_{0.5}O_{6-\delta}$-SDC anode under a constant current load of 540mA cm^{-2} in H_2 (3 vol% H_2O) at 800°C.

in the anodes. Extracting all Ni from $Sr_{1.9}Fe_{1.4}Ni_{0.1}Mo_{0.5}O_{6-\delta}$ only yields 1 wt% of Ni in the anode and considering the observation of Ni-Fe alloy the portion of reduced metal Ni should be even smaller for $Sr_{1.9}Fe_{1.4}Ni_{0.1}Mo_{0.5}O_{6-\delta}$ in this work. Additionally, the formation of alloy may also result in different catalytic activity comparing with the single metal phase.

Stability of $Sr_{1.9}Fe_{1.4}Ni_{0.1}Mo_{0.5}O_{6-\delta}$-SDC was investigated by operating the fuel cell under a constant current load in H_2 at 800°C. The voltage dependence on time is shown in Figure 8. Similar to other material systems which can generate nano metal particles upon reduction in anode conditions, a gradual increase in cell performance was observed in the first 60 h for the $Sr_{1.9}Fe_{1.4}Ni_{0.1}Mo_{0.5}O_{6-\delta}$-SDC anode, probably due to the accumulation of metal catalysts on the surface. After reaching the maximum cell power output, the cell performance degraded at a very low rate. Similar degradation behavior was also reported for $La_{0.8}Sr_{0.2}Cr_{1-y}X_yO_3$, X = Ni and Ru, and Ni in which a high coarsening rate of the nanosized metal particles was thought to cause the performance degradation.[16] However, the furry surface on the reduced $Sr_{1.9}Fe_{1.4}Ni_{0.1}Mo_{0.5}O_{6-\delta}$ as well as the formation of alloy may account for the slower degradation rate observed in this study for inhibiting the growth of metal particles.

Impedance spectra of the cell before and after the galvanostatic cell test were recorded under open circuit conditions in H_2 and the Nyquist plots are shown in Figure 9. It can be seen that the high frequency arc decreased slightly while the low frequency arc increased slightly

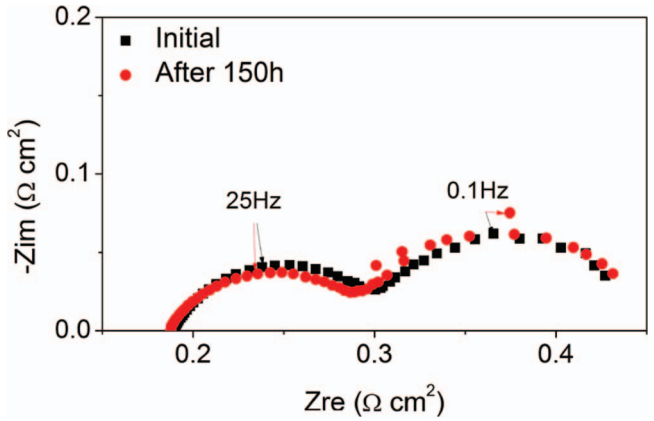

Figure 9. Nyquist plots of a single cell with $Sr_{1.9}Fe_{1.4}Ni_{0.1}Mo_{0.5}O_{6-\delta}$-SDC anode before and after the galvanostatic test.

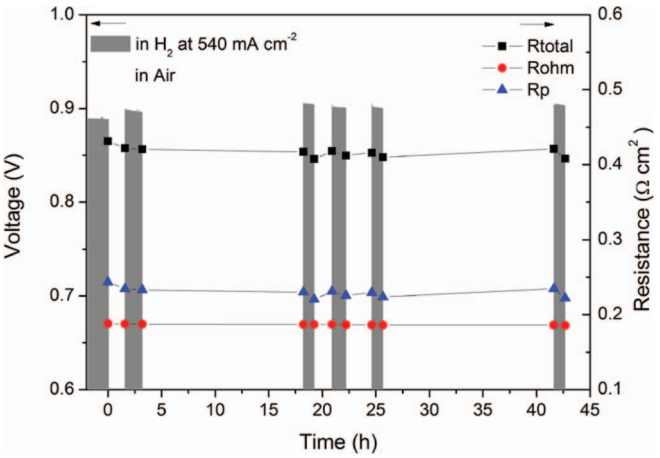

Figure 10. Cell voltage and resistance of $Sr_{1.9}Fe_{1.4}Ni_{0.1}Mo_{0.5}O_{6-\delta}$-SDC anode versus time during redox cycling at 800°C.

after the test. As long as the metal alloy gradually accumulated on the surface in H_2, the H_2 adsorption/desorciation and charge transfer may be further facilitated. This may account for the decrease of the high frequency polarization resistance. For the enlarged low frequency arc in the impedance spectra, it may be related to the coarsening of metal particles as reported for other material systems.[16,18] Another possible reason may be the blockage of gas diffusion passages by Sr-riched phase from reduction. However, the overall change in the impedance spectra after the stability test was subtle, indicating good cell performance stability of the composite anode.

Redox stability of $Sr_{1.9}Fe_{1.4}Ni_{0.1}Mo_{0.5}O_{6-\delta}$-SDC anode was investigated at 800°C by switching the fuel gas between H_2 and air. After each cycle, the fuel cell was operated under a galvanostatic condition in H_2 for about 1 h and the impedance spectra were recorded. The change on time of cell voltage and resistances determined from the impedance spectra during five redox cycles are shown in Figure 10. It can be observed that the cell voltage in H_2 under a current load was even improved after 5 cycles when compared with the initial value. During two of the redox cycles, the anode was exposed to air for almost 20 h but the cell performance was found not sensitive to the anode exposure time in air. From the resistance results shown in Figure 10, it can be also seen that the major change was from the polarization resistance which also dominated the overall cell impedance while the ohmic resistance wasn't affected by the redox cycling. The polarization resistance decreased after the fuel cell being operated in H_2 for 1 h in each cycle, indicating the re-established metal phase plays an important role in improving the single cell performance. Obviously, the polarization resistance decreased after five redox cycles as shown in Figure 10. It was consistent with those reported elsewhere that the redox cycling may help regenerating the nano-sized metal phase on the ceramic oxide.[18] Generally speaking, $Sr_{1.9}Fe_{1.4}Ni_{0.1}Mo_{0.5}O_{6-\delta}$-SDC anode showed excellent stability during redox cycling.

Since Ni-Fe anode has been demonstrated to have good performance in propane,[29] the anode performance of $Sr_{1.9}Fe_{1.4}Ni_{0.1}Mo_{0.5}O_{6-\delta}$-SDC in propane was also investigated. The initial cell peak power density only reached 227 mW cm^{-2} at 800°C as shown in Figure 11a. A huge low frequency arc was observed in the impedance spectra in Figure 11b, indicating that the cell performance was limited by gas diffusion. The cell was operated under a current load of 300 mA cm^{-2} for about 18 h and a substantial amount of liquid oil products was detected at the anode exhaust outlet. These longer chain hydrocarbons may be produced by dehydrogenation of propane in the anode, implying that the anode was not active enough to fully oxidize propane. Interestingly, the OCV was improved from 1.08 V to 1.14 V temporarily after the galvanostatic test and cell performance were. Similar phenomenon in propane has also been reported for

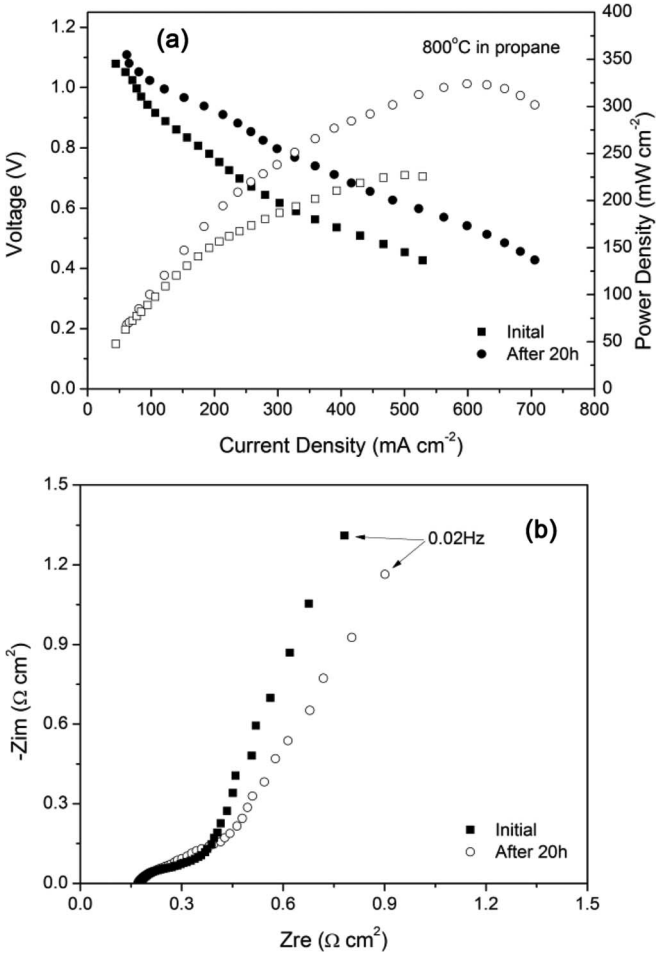

Figure 11. (a) I-V and I-P curves, (b) Nyquist plots of $Sr_{1.9}Fe_{1.4}Ni_{0.1}Mo_{0.5}O_{6-\delta}$-SDC anode in propane (3 vol% H_2O).

other anode materials.[29] The cell peak power density reached 324 mW cm^{-2}. The cell power output is still much lower than the Ni-Fe anode reported in the literature probably due to the low content of the metal catalysts generated on $Sr_{1.9}Fe_{1.4}Ni_{0.1}Mo_{0.5}O_{6-\delta}$-SDC anode.[29]

Conclusions

Ni-Fe alloy nano particles were generated on the $Sr_{1.9}Fe_{1.4}Ni_{0.1}Mo_{0.5}O_{6-\delta}$ anode under the SOFC operating conditions. This composition showed sufficient electrical conductivity as an SOFC anode. Due to the improved catalytic activity by the metal particles, $Sr_{1.9}Fe_{1.4}Ni_{0.1}Mo_{0.5}O_{6-\delta}$-SDC anode showed excellent cell performance in H_2 and its performance was quite stable. The anode performance of $Sr_{1.9}Fe_{1.4}Ni_{0.1}Mo_{0.5}O_{6-\delta}$-SDC can also be regenerated upon redox cycling and $Sr_{1.9}Fe_{1.4}Ni_{0.1}Mo_{0.5}O_{6-\delta}$ has excellent redox stability. $Sr_{1.9}Fe_{1.4}Ni_{0.1}Mo_{0.5}O_{6-\delta}$-SDC anode also showed reasonable cell performance when propane was used as fuel. This study indicates that $Sr_{1.9}Fe_{1.4}Ni_{0.1}Mo_{0.5}O_{6-\delta}$ is a very promising alternative anode material with enhanced catalytic activity and excellent redox stability inherited from the parent material $Sr_2Fe_{1.5}Mo_{0.5}O_{6-\delta}$ for solid oxide fuel cells.

Acknowledgment

We're grateful for the financial support from National Science Foundation (DMR-1210792), the HeteroFoaM Center, an Energy Frontier Research Center funded by the U.S. Department of Energy, Office of Science, Office of Basic Energy Sciences (DE-SC0001061), the 973 Project (2012CB215404) and the NSFC (51261120378). The authors acknowledge Dr. Dong Su of Brookhaven National Laboratory and Hsin-Hui (Sonia) Huang of University of New South Wales for the assistance in TEM work.

References

1. S. W. Tao and J. T. S. Irvine, *Nat. Mater.*, **2**, 320 (2003).
2. O. A. Marina, N. L. Canfield, and J. W. Stevenson, *Solid State Ionics*, **149**, 21 (2002).
3. S. Hui and A. Petric, *J. Eur. Ceram. Soc.*, **22**, 1673 (2002).
4. T. Kolodiazhnyi and A. Petric, *J. Electroceram.*, **15**, 5 (2005).
5. Y. Huang, R. I. Dass, Z. Xing, and J. B. Goodenough, *Science*, **312**, 254 (2006).
6. Q. Liu, X. Dong, G. Xiao, F. Zhao, and F. Chen, *Adv. Mater.*, **22**, 5478 (2010).
7. G. Xiao, Q. Liu, X. Dong, K. Huang, and F. Chen, *J. Power Sources*, **195**, 8071 (2010).
8. L. Zhang, Q. Zhou, Q. He, and T. He, *J. Power Sources*, **195**, 6356 (2010).
9. T. Wei, Q. Zhang, Y. Huang, and J. B. Goodenough, *J. Mater. Chem.*, **22**, 225 (2012).
10. X. Zhu, Z. Lu, B. Wei, K. Chen, M. Liu, X. Huang, and W. Su, *J. Power Sources*, **190**, 326 (2009).
11. Q. Ma, F. Tietz, A. Leonide, and E. Ivers-Tiffee, *Electrochem. Commun.*, **12**, 1326 (2010).
12. B. Smith and M. Gross, *Electrochemical and Solid State Letters*, **14**, B1 (2011).
13. G. Xiao and F. Chen, *Electrochem. Commun.*, **13**, 57 (2011).
14. G. Xiao, C. Jin, Q. Liu, A. Heyden, and F. Chen, *J. Power Sources*, **201**, 43 (2012).
15. B. D. Madsen, W. Kobsiriphat, Y. Wang, L. D. Marks, and S. A. Barnett, *J. Power Sources*, **166**, 64 (2007).
16. W. Kobsiriphat, B. D. Madsen, Y. Wang, M. Shah, L. D. Marks, and S. A. Barnett, *J. Electrochem. Soc.*, **157**, B279 (2010).
17. S. Boulfrad, M. Cassidy, and J. T. S. Irvine, *Solid State Ionics*, **197**, 37 (2011).
18. D. M. Bierschenk, E. Potter-Nelson, C. Hoel, Y. Liao, L. Marks, K. R. Poeppelmeier, and S. A. Barnett, *J. Power Sources*, **196**, 3089 (2011).
19. C. Yang, Z. Yang, C. Jin, G. Xiao, F. Chen, and M. Han, *Adv. Mater.*, **24**, 1439 (2012).
20. G. C. Kostogloudis and C. Ftikos, *Solid State Ionics*, **126**, 143 (1999).
21. A. Mai, V. A. C. Haanappel, S. Uhlenbruck, F. Tietz, and D. Stover, *Solid State Ionics*, **176**, 1341 (2005).
22. G. Xiao, Q. Liu, S. Wang, V. G. Komvokis, M. D. Amiridis, A. Heyden, S. Ma, and F. Chen, *J. Power Sources*, **202**, 63 (2012).
23. A. B. Munoz-Garcia, D. E. Bugaris, M. Pavone, J. P. Hodges, A. Huq, F. L. Chen, H. C. zur Loye, and E. A. Carter, *J. Am. Chem. Soc.*, **134**, 6826 (2012).
24. L. dos Santos-Gomez, L. Leon-Reina, J. M. Porras-Vazquez, E. R. Losilla, and D. Marrero-Lopez, *Solid State Ionics*, **239**, 1 (2013).
25. D. Golberg, C. Gu, Y. Bando, M. Mitome, and C. Tang, *Acta Mater.*, **53**, 1583 (2005).
26. A. A. Markov, I. A. Leonidov, M. V. Patrakeev, V. L. Kozhevnikov, O. A. Savinskaya, U. V. Ancharova, and A. P. Nemudry, *Solid State Ionics*, **179**, 1050 (2008).
27. G. Xiao, Q. Liu, S. Nuansaenga, and F. Chen, *ECS Trans.*, **45**, 355 (2012).
28. B. He, L. Zhao, S. Song, T. Liu, F. Chen, and C. Xia, *J. Electrochem. Soc.*, **159**, B619 (2012).
29. T. H. Shin, S. Ida, and T. Ishihara, *J. Am. Chem. Soc.*, **133**, 19399 (2011).